

All-optical grating in a $V + \Xi$ configuration using a Rydberg state

Forough Bozorgzadeh* and Mostafa Sahrai

Research Institute for Applied Physics and Astronomy, University of Tabriz, Tabriz, Iran

(Received 23 July 2018; published 10 October 2018)

We present a theoretical model for controlling the Fraunhofer diffraction patterns of a weak probe field passing through an atomic vapor. In this model a Rydberg state is taken as the uppermost level. The proposed system contains a combined two well-known V - and Ξ -type configurations which are exposed to a weak probe field and two control fields. The position-dependent feature of the atom-field interaction leads to the periodic transmission spectrum, and various Fraunhofer diffraction patterns are obtained due to the all-optical grating. Also, it is shown that the intensity of the higher-order diffraction can be controlled by tuning the coupling field intensity and the interaction length.

DOI: [10.1103/PhysRevA.98.043822](https://doi.org/10.1103/PhysRevA.98.043822)**I. INTRODUCTION**

Rydberg atoms have achieved considerable attention due to their huge electric-dipole moments, very long radiative lifetimes [1], large extensions of the electronic wave functions [2], and extreme sensitivity to external electric fields [3]. Rydberg atoms are directly created by laser excitations or coherently by stimulated Raman rapid adiabatic passage [4]. The strong interacting nature of Rydberg atoms makes them a suitable medium for engineering long-range interactions, long-range quantum information processing [5], investigating the strongly correlated systems [6,7], or even engineering the exotic quantum many-body phases [8,9].

The large dipole moment, the long radiative lifetime, and very weak binding energies of the Rydberg atoms make them attractive candidates for studying the quantum optics phenomena [10]. Also, some physical properties of the medium, such as geometric cross section, can be changed due to the huge size of the Rydberg atoms [11]. Therefore, these atoms are extremely sensitive to the applied external electromagnetic fields. Basically, manipulation of the Rydberg atoms with small gradients of electric fields is possible due to their huge electric dipole-dipole interactions. Long-range dipole-dipole interactions in the Rydberg atoms can exceed several micrometers, leading to many-body effects [12,13]. Highly excited Rydberg atoms with long-range interparticle interactions have various applications in complex quantum systems, such as solid-state physics and plasma physics. The applications of these strong interactions range from photoassociation (PA) [14] to energy transfer in biological molecules [15]. For example, Rydberg atoms are a suitable building block for studying N -body, many-body cooperative, or collective effects [16,17]. These atoms are employed to quantum engineering of the entanglement of natural particles [18] and implementing the fast quantum gates [19,20]. Also, during light storage, controllable two-photon states are generated by using the interactions between Rydberg atoms [21].

On the other hand, electromagnetically induced transparency (EIT) refers to the cancellation of a weak probe laser field absorption due to the destructive quantum interference via a strong coupling laser. Coherent coupling of the Rydberg states via EIT is used to generate cross-phase modulation (XPM) [22] and photon entanglement. It is well known that by using a standing-wave pattern instead of the traveling wave in a typical EIT system, the probe field experiences periodic spatial variations of absorption and dispersion, and the medium can act as an amplitude or phase grating. This electromagnetically induced grating (EIG) can effectively diffract the probe field into higher orders of diffraction. EIG has various applications in optical communications, such as probing the optical characteristics of the materials [23], realization of optical bistability [24], nonlinear multiwave mixing [25], surface solitons [26], all-optical switching, routing, and light storage [27,28]. So far, the EIG has been theoretically realized in the Λ -type [29], Ξ -type [30,31], N -type [23], Y -type [32], semiconductor quantum-well systems [33], and has experimentally been observed in cold [34,35] and hot [36] atomic samples. Recently, the effect of EIG is proposed in Rydberg atoms [37] in a three-level cascade system.

In this paper, we present the details about the realization of diffraction gratings in a four-level ($V + \Xi$) atomic system involving a Rydberg state as the uppermost level. It is shown that the far-field (or Fraunhofer) diffraction patterns are strongly influenced by the Rabi frequency of the standing-wave field and the interaction length of the atomic sample. It is well known that giant optical nonlinearities, and ultimately the regime of strong atom-photon interaction, can be achieved using EIT schemes with a Rydberg state [38,39]. Thus, the use of a Rydberg state provides an opportunity to realize more practical all-optical gratings by establishing the EIT condition. Furthermore, the presence of additional levels allows the use of additional control fields, which leads to the modification of the EIT window. In particular, the combination of V and Ξ systems provides more efficient all-optical grating using a Rydberg state. Among many proposals, this configuration has been utilized to study, of the electromagnetically

*fbozorgzadeh@tabrizu.ac.ir

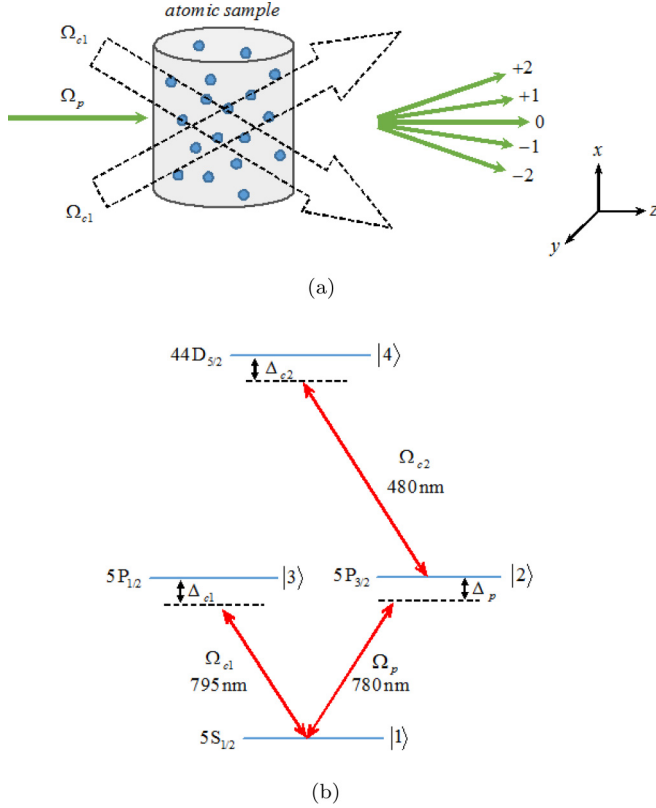


FIG. 1. (a) Schematics of the cold atoms interacting with probe and standing-wave field. (b) Energy-level configuration for a four-level ($V + \Xi$) system.

induced absorption (EIA) resonances [40], sub- and superluminal light propagation [41], optical bistability [42], and atom localization [43].

This paper is organized as follows: In Sec. II we present the theoretical model and the governing equations. In Sec. III, by using a standing-wave coupling field, we investigate the spatial modulation of the absorption and dispersion to obtain the far-field diffraction patterns. We present the conclusion in Sec. IV.

II. MODEL AND EQUATIONS

The schematics of the proposed system is shown in Fig. 1. We consider the energy levels of the cold ^{87}Rb atoms with level $|1\rangle \equiv 5S_{1/2}|F=1\rangle$ as a ground state, level $|4\rangle \equiv 44D_{5/2}$

as a Rydberg state, and the other two intermediate levels are $|2\rangle \equiv 5P_{3/2}|F=2\rangle$ and level $|3\rangle \equiv 5P_{1/2}|F=2\rangle$. The Ξ -type configuration is formed by a probe light field with Rabi frequency Ω_p acting on a $|1\rangle \rightarrow |2\rangle$ transition and a strong control field with Rabi frequency Ω_{c2} acting on $|2\rangle \rightarrow |4\rangle$. However, the V -type configuration involves the above-mentioned probe field and a standing-wave coupling field with Rabi frequency Ω_{c1} that drives $|1\rangle \rightarrow |3\rangle$ transition. The corresponding decay rates are $\Gamma_1 = 0$ (since level $|1\rangle$ is ground state), $\Gamma_2 = 2\pi \times 6.1$ MHz, $\Gamma_3 = 2\pi \times 5.9$ MHz, and $\Gamma_4 = 2\pi \times 0.3$ MHz. Note that other states (e.g., S or D) can also be chosen by tuning the laser field frequency and polarization, as well as applying the appropriate selection rules [44,45]. In addition, for the highly excited state ^{85}Rb or ^{87}Rb , only the remarkable fine interaction ($nD_{3/2}$ and $nD_{5/2}$) remains, and the nd state hyperfine splitting may be neglected [46,47]. At low pumping intensities, the Rydberg signal for $44D_{5/2}$ is stronger than that of $44D_{3/2}$ [45]. For the ground and the intermediate states, the states are chosen so that the decay rates to some other lower levels become zero. Thus the branching ratio for the selected levels are unity. Also, since the ground electronic state of the ^{87}Rb is $5s^2 S_{1/2}$, the relaxation to the lower filled states is not allowed.

We assume the standing-wave field has a sinusoidal profile as $\Omega_{c1} = \Omega_{c1} \sin(\pi x / \Lambda_{cx})$, where Λ_{cx} is the spatial frequency of the standing wave. Also, the center of mass of the atoms is nearly constant along the standing-wave field. Thus, the kinetic energy of the atoms can be neglected by applying the Raman-Nath approximation. It is assumed that the Rydberg gas is so cold that the spatial positions of the atoms will not be changed due to the spatially modulated standing wave. Therefore, the interaction Hamiltonian of the system under the electric-dipole approximation and in rotating-wave approximation can be written as

$$H_I = \frac{\hbar}{2} [\Omega_p |1\rangle\langle 2| + \Omega_{c1} |1\rangle\langle 3| + \Omega_{c2} |2\rangle\langle 4|] + \text{H.c.} \\ + \hbar [\Delta_p |2\rangle\langle 2| + \Delta_{c1} |3\rangle\langle 3| + (\Delta_p + \Delta_{c2}) |4\rangle\langle 4|], \quad (1)$$

where $\Delta_p = \omega_{21} - \nu_p$, $\Delta_{c1} = \omega_{31} - \nu_{c1}$, $\Delta_{c2} = \omega_{42} - \nu_{c2}$ are the corresponding frequency detunings. Here, ν_p , ν_{c1} , and ν_{c2} stand for the frequency of probe, coupling, and standing-wave fields, respectively. In addition, ω_{ij} ($i, j = 1, 2, 3$, and 4) are the frequency difference between level $|i\rangle$ and level $|j\rangle$.

The time evolution of the density-matrix equations of motion is given by

$$\frac{\partial \rho_{11}}{\partial t} = \Gamma_2 \rho_{22} + \Gamma_3 \rho_{33} + \frac{i}{2} \Omega_p (\rho_{12} - \rho_{21}) + \frac{i}{2} \Omega_{c1} \sin(\pi x / \Lambda_{cx}) (\rho_{13} - \rho_{31}), \\ \frac{\partial \rho_{22}}{\partial t} = -\Gamma_2 \rho_{22} + \Gamma_4 \rho_{44} + \frac{i}{2} \Omega_p (\rho_{21} - \rho_{12}) + \frac{i}{2} \Omega_{c2} (\rho_{24} - \rho_{42}), \\ \frac{\partial \rho_{33}}{\partial t} = -\Gamma_3 \rho_{33} + \frac{i}{2} \Omega_{c1} \sin(\pi x / \Lambda_{cx}) (\rho_{31} - \rho_{13}), \\ \frac{\partial \rho_{44}}{\partial t} = -\Gamma_4 \rho_{44} + \frac{i}{2} \Omega_{c2} (\rho_{42} - \rho_{24}), \\ \frac{\partial \rho_{12}}{\partial t} = \left(-\frac{\Gamma_2}{2} + i \Delta_p \right) \rho_{12} + \frac{i}{2} \Omega_p (\rho_{11} - \rho_{22}) - \frac{i}{2} \Omega_{c1} \sin(\pi x / \Lambda_{cx}) (\rho_{32} - \rho_{14}),$$

$$\begin{aligned}
\frac{\partial \rho_{13}}{\partial t} &= \left(-\frac{\Gamma_3}{2} + i\Delta_{c1} \right) \rho_{13} + \frac{i}{2} \Omega_{c1} \sin(\pi x / \Lambda_{cx}) (\rho_{11} - \rho_{33}) - \frac{i}{2} \Omega_p \rho_{23}, \\
\frac{\partial \rho_{14}}{\partial t} &= \left[-\frac{\Gamma_4}{2} + i(\Delta_p + \Delta_{c2}) \right] \rho_{14} - \frac{i}{2} \Omega_p \rho_{24} - \frac{i}{2} \Omega_{c1} \sin(\pi x / \Lambda_{cx}) \rho_{34} + \frac{i}{2} \Omega_{c2} \rho_{12}, \\
\frac{\partial \rho_{23}}{\partial t} &= \left[-\frac{1}{2}(\Gamma_2 + \Gamma_3) + i(\Delta_{c1} - \Delta_p) \right] \rho_{23} - \frac{i}{2} \Omega_p \rho_{13} - \frac{i}{2} \Omega_{c2} \rho_{43} + \frac{i}{2} \Omega_{c1} \sin(\pi x / \Lambda_{cx}) \rho_{21}, \\
\frac{\partial \rho_{24}}{\partial t} &= \left[-\frac{1}{2}(\Gamma_2 + \Gamma_4) + i\Delta_{c2} \right] \rho_{24} + \frac{i}{2} \Omega_{c2} (\rho_{22} - \rho_{44}) - \frac{i}{2} \Omega_p \rho_{14}, \\
\frac{\partial \rho_{34}}{\partial t} &= \left[-\frac{1}{2}(\Gamma_3 + \Gamma_4) + i(\Delta_p - \Delta_{c1} + \Delta_{c2}) \right] \rho_{34} - \frac{i}{2} \Omega_{c1} \sin(\pi x / \Lambda_{cx}) \rho_{14} + \frac{i}{2} \Omega_{c2} \rho_{32}. \tag{2}
\end{aligned}$$

The above density matrix elements obey the normalization and Hermitian condition $\sum_{i=1}^4 \rho_{ii} = 1$ and $\rho_{ij} = \rho_{ji}^*$.

The atom-field interaction of the system is described by the electric susceptibility χ_p . The susceptibility of probe field can be calculated by solving the above density matrix equations under the steady-state condition ($\frac{\partial}{\partial t} \rightarrow 0$) and in the weak probe field approximation. In this regime, i.e., $\Omega_p \ll \Gamma_2$, the perturbation approach can be applied. Thus, the linear electric susceptibility depends on the coherence term ρ_{21} via equation

$$\chi_p = \frac{N |\hat{\mu}_{21}|^2}{\epsilon_0 \hbar \Omega_p} \rho_{21}, \tag{3}$$

where

$$\rho_{21} = -\frac{1}{8A} i \Omega_p \times [(\Omega_{c2}^2 + 4\gamma_{32}\gamma_{34})\gamma_{14} + \gamma_{32} \Omega_{c1}^2 \sin^2(\pi x / \Lambda_{cx})], \tag{4}$$

and

$$\begin{aligned}
A &= -\frac{1}{16} \Omega_{c1}^4 \sin^4(\pi x / \Lambda_{cx}) \\
&\quad - \frac{1}{16} \Omega_{c1}^3 \sin^3(\pi x / \Lambda_{cx}) \Omega_{c2} \\
&\quad + \frac{1}{16} \Omega_{c1}^2 \sin^2(\pi x / \Lambda_{cx}) (\Omega_{c2}^2 + 4\gamma_{12}\gamma_{32} - 4\gamma_{14}\gamma_{34}) \\
&\quad + \frac{1}{16} \Omega_{c1} \sin(\pi x / \Lambda_{cx}) (\Omega_{c2}^3 + 4\Omega_{c2}\gamma_{32}\gamma_{34}) \\
&\quad + \frac{1}{4} \gamma_{12}\gamma_{14} (\Omega_{c2}^2 + 4\gamma_{32}\gamma_{34}), \\
\gamma_{12} &= -\left(\frac{\Gamma_2}{2} - i\Delta_p \right), \\
\gamma_{32} &= -\frac{1}{2}(\Gamma_2 + \Gamma_3) + i(\Delta_{c1} - \Delta_p), \\
\gamma_{34} &= -\frac{1}{2}(\Gamma_3 + \Gamma_4) - i(\Delta_p - \Delta_{c1} + \Delta_{c2}), \\
\gamma_{14} &= -\frac{1}{2}\Gamma_4 - i(\Delta_p + \Delta_{c1}). \tag{5}
\end{aligned}$$

Here, N is the atom number density and $\hat{\mu}_{21}$ is the matrix element of the electric-dipole moment for probe transition. As a result of intensity-dependent susceptibility, a strong coupling field with a standing-wave pattern may lead to spatially modulated absorption and dispersion. Thus, the ensemble can

act as an atomic grating, which can diffract the weak probe light into higher orders of diffraction.

In order to study the diffraction patterns of the probe light, we begin with Maxwell's wave equation. As shown in Fig. 1(a), the weak probe field with amplitude E_p propagates along the z direction through an atomic sample of length L . Under the slowly varying envelope approximation (SVEA), and in the steady-state regime, the spatial behavior of the weak probe field can be described by [29]

$$\frac{\partial E_p}{\partial z} = i \frac{\pi}{\epsilon_0 \lambda_p} P_p, \tag{6}$$

where λ_p is the wavelength of the weak probe field. For experimental realization of the proposed EIG, a thin vapor cell containing cold ^{87}Rb atoms is preferred. This condition requires a high optical depth of the medium. However, increasing the optical depth by increasing the atomic density is problematic, because if the interatomic spacing becomes comparable to the size of the electron orbit, then additional dephasing occurs as a result of the interactions between ground-state atoms and Rydberg electrons [48]. In a recent technique for laser cooling in an EIT experiment, an ensemble of cold atoms with an optical depth exceeding 500 has been reported in different Rb isotopes [49]. Hence, the assumption of thin grating is rational.

Substituting the slowly varying induced polarization $P_p = \epsilon_0 \chi_p E_p = 2N(\hat{\mu}_{21}\rho_{21} + \hat{\mu}_{12}\rho_{12})$ into Eq. (6), and by choosing Λ_{cx} as a unit of x and $z_0 = 2\lambda_p \hbar \epsilon_0 \Gamma_{20} / \pi N \hat{\mu}_{21}^2$ as the unit of z , the normalized transmission function of the probe field for an interaction length L of the medium can be obtained as

$$\begin{aligned}
T(x) &= e^{-\text{Im}(\chi_p) L} e^{i \text{Re}(\chi_p) L} \\
&\equiv e^{-\alpha(x)L} e^{i\phi(x)}, \tag{7}
\end{aligned}$$

where the first (second) term in the exponential corresponds to the atomic grating absorption (phase) modulations, which are given by

$$|T(x)| = |e^{-\text{Im}(\chi_p) L}| \tag{8}$$

and

$$\phi(x) = \text{Re}(\chi_p) L. \tag{9}$$

TABLE I. Corresponding parameters for the optical properties of Rydberg ^{87}Rb transitions.

Level	Rb state	$\Gamma/2\pi$ (MHz)	Wavelength (nm)
1⟩	$5S_{1/2}$	0 (Ground state)	0
2⟩	$5P_{3/2}$	6.1	$\lambda_p = 780$
3⟩	$5P_{1/2}$	5.9	$\lambda_{c1} = 795$
4⟩	$44D_{5/2}$	0.3	$\lambda_{c2} = 480$

By taking the Fourier transformation of $T(x)$, we obtain the far-field or Fraunhofer diffraction as

$$I_p(\theta) = |F(\theta)|^2 \frac{\sin^2(M\pi \Lambda_{cx} \sin \theta / \lambda_p)}{M^2 \sin^2(\pi \Lambda_{cx} \sin \theta / \lambda_p)}. \quad (10)$$

Here, the weak probe field is chosen as a plane wave, M denotes the number of the spatial periods of the atomic grating illuminated by the probe field, and θ denotes the diffraction angle of probe field along the x direction with respect to the z direction. So, the parameter $F(\theta) = \int_0^1 T(x) \exp(-i2\pi \Lambda_{cx} x \sin \theta / \lambda_p) dx$ represents the Fraunhofer diffraction of a single space period. The n th-order diffraction is determined by the grating equation, i.e., $\sin \theta = n\lambda_p / \Lambda_{cx}$. Hence, the first- and second-order diffraction intensity can be expressed as

$$I_p(\theta_1) = |F(\theta_1)|^2 = \left| \int_0^1 T(x) \exp(-i2\pi x) dx \right|^2 \quad (11)$$

and

$$I_p(\theta_2) = |F(\theta_2)|^2 = \left| \int_0^1 T(x) \exp(-i4\pi x) dx \right|^2. \quad (12)$$

III. RESULTS AND DISCUSSION

In this section, the effect of system and laser field parameters on the diffraction feature of the proposed four-level ($\Xi + V$) atomic system is investigated. A low-power diode laser can be used as the weak probe field to monitor the $5S_{1/2} \rightarrow 5P_{3/2}$ transition. For this purpose, Eq. (2) is solved in the steady state with the actual parameters of a cold ^{87}Rb atomic system that is compatible for experimental realization. The electric dipole moment for the $|1\rangle \rightarrow |2\rangle$ transition is $\hat{\mu}_{21} = 3.58 \times 10^{-29}$ C m. The corresponding atomic system parameters are summarized in Table I. For numerical calculations, it is assumed that the probe laser field is weak, i.e., $N|\hat{\mu}_{21}|^2 / \hbar \epsilon_0 \Omega_p \approx 1$. From an experimental point of view, all the mentioned wavelengths are available with the aid of diode laser systems.

A. Absorption profiles

Since the electric susceptibility plays a crucial role in electromagnetically induced grating, first in Fig. 2 we plot the absorption and dispersion of the probe field as a function of the probe detuning. It is assumed that the control and coupling fields are in resonance with the corresponding transitions, i.e., $\Delta_{c1} = \Delta_{c2} = 0$. Figures 2(a) and 2(b) show the results for imaginary (absorption) and real (dispersion) part of the electric susceptibility for the fixed Rabi frequency of coupling

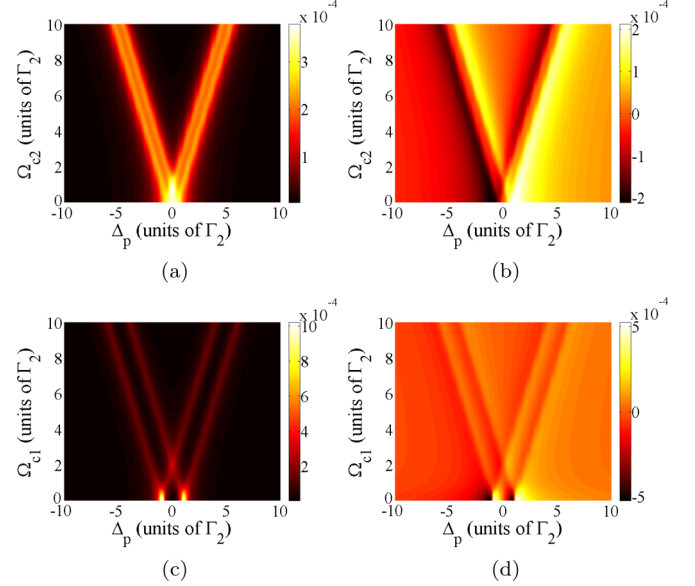


FIG. 2. (a) Probe absorption and (b) dispersion for fixed $\Omega_{c2} = 2\Gamma_2$, and (c) probe absorption and (d) dispersion for fixed $\Omega_{c1} = 1\Gamma_2$. The other parameters are $\Delta_{c1} = \Delta_{c2} = 0$, $N = 3 \times 10^{10}$ atom/cm $^{-3}$, $\hat{\mu}_{21} = 3.58 \times 10^{-29}$ C m, $x = 2$, and $\Lambda_{cx} = 4$.

field, i.e., $\Omega_{c1} = 1\Gamma_2$. The Rabi frequency of the control field (Ω_{c2}) and the probe field detuning are varied in the range of $0 : 10\Gamma_2$ and $-10\Gamma_2 : 10\Gamma_2$, respectively. It is obvious that in the absence of Ω_{c2} , an absorption peak appears that corresponds to the absorption of a typical V-type system. By increasing the Ω_{c2} , this absorption peak splits into two peaks and the system experiences a Rydberg EIT effect. The corresponding dispersion diagram is shown in Fig. 2(b). From Fig. 2(c) it is clear that for $\Omega_{c1} = 0$ and a fixed control intensity Ω_{c2} , i.e., a simple Ξ -type system, the probe field experiences a Rydberg EIT effect in the locations of the dressed states which is created by the control field, i.e., $\Delta_p = \pm \Omega_{c2}/2$. This is to say, the absorption profile splits into an Autler-Townes doublet. It is observed that the width of EIT windows is proportional to the Rabi frequency of the control field and higher intensities result in wider EIT windows. Moreover, by increasing the Rabi frequency of the coupling field Ω_{c1} , each of these absorption peaks splits into two peaks. The corresponding dispersion diagram is shown in Fig. 2(d).

B. Absorption grating

As it mentioned before, the coupling field with a standing-wave pattern can lead to spatial amplitude and phase modulation across the profile of the probe field. This periodic change manifests itself in the transmission function of the probe field. It can be seen from Eqs. (8) and (9) that the absorptive (or dispersive) part of the electric susceptibility contributes in the amplitude (or phase) of transmission function. According to Fig. 3, in the resonance condition, i.e., $\Delta_p = 0$, the dispersion of the medium becomes zero, while the amplitude of the transmission function is almost unity. In Figs. 3(a) and 3(d), it is assumed that the Rabi frequency of the coupling field is zero; therefore the results show the behavior of a typical Ξ -type system. Although the transmission of the medium is

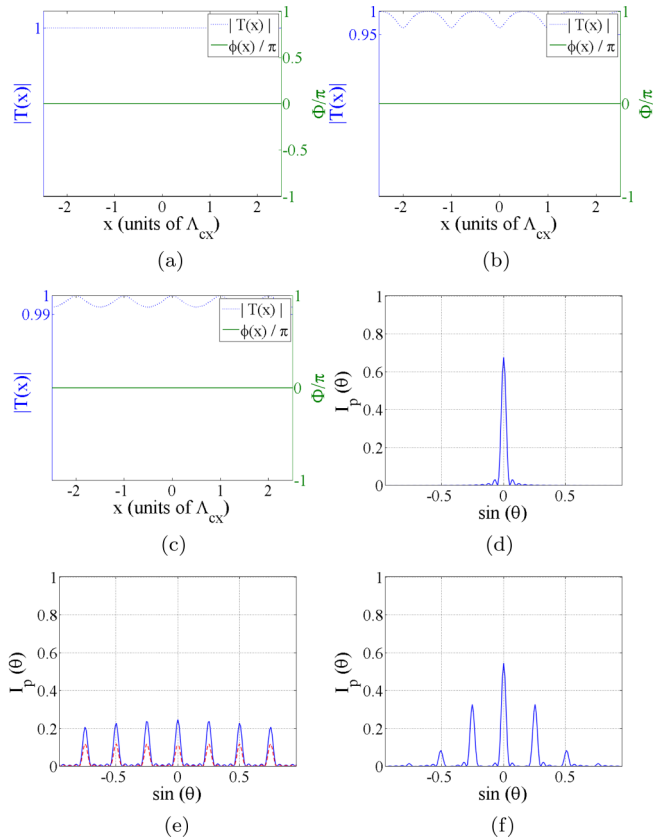


FIG. 3. *Absorption grating*: The amplitude $|T(x)|$ and the phase ϕ/π of the transmission function vs x for (a) $\Omega_{c1} = 0, \Omega_{c2} = 2\Gamma_2$; (b) $\Omega_{c1} = 1\Gamma_2, \Omega_{c2} = 0$; (c) $\Omega_{c1} = 1\Gamma_2, \Omega_{c2} = 2\Gamma_2$. (d)–(f) Corresponding normalized diffraction intensity for on-resonance condition, i.e., $\Delta_p = \Delta_{c1} = \Delta_{c2} = 0$. Common parameters are $\Lambda_{cx} = 4, M = 5$, and $L = 50$.

almost unity due to the Rydberg-EIT effect, no diffraction pattern is observed. From Fig. 3(d), it is obvious that all of the probe light energy will gather in the zeroth order of the diffraction and no grating is formed, which is a reasonable result since a standing-wave coupling field is necessary for the formation of all-optical grating.

Figures 3(b) and 3(e) show the results for a typical V -type system. In such a system, the EIT significantly differs from a Ξ -type or Λ -type system. In a V -type system, the coupling field modifies the population of the ground state which is also coupled to the probe field, so a saturation phenomenon might take place. Thus, the absorption profile is simultaneously influenced by the EIT and saturation effects. This saturation leads to the increment of the absorption at the resonance ($\Delta_p = 0$) and does not affect the width of the transparency windows arising from the EIT effect [50]. Figure 3(b) shows the amplitude and phase of the transmission function for the parameters $\Omega_{c1} = 1\Gamma_2, \Omega_{c2} = 0$, and $\Delta_p = \Delta_{c1} = \Delta_{c2} = 0$. A small absorption modulation which oscillates around the average transmission of 98% is observed for the probe field and the phase part is still zero. The spatially modulated coupling field generates the periodic regions of high and low probe absorption, which diffracts the weak probe field. The corresponding diffraction spectrum is shown in Fig. 3(e).

The red-dashed line corresponds to the Ξ -type system when the standing-wave field applies to the $|2\rangle \rightarrow |4\rangle$ transition. Thus, we expect that for a combined V and Ξ system, the intensity of the diffraction orders and consequently the diffraction efficiency is enhanced. In Figs. 3(c) and 3(f), the results for a four-level ($V + \Xi$) atomic system involving a Rydberg state as the uppermost level are shown. Due to the Rydberg-EIT effect and the periodic modulation of the transmission function, the all-optical induced grating acts as a pure absorption grating with maximal transmission. As it is well-known, the diffraction efficiency is defined as the ratio of the intensities of the chosen order of diffracted beam and the incident beam. A pure absorption grating is generally less efficient than a phase grating. For considerable enhancement of the diffraction efficiency of the probe field, one needs to find regimes with large phase modulation in nearly transparent medium. High transparency is provided by the Rydberg-EIT effect in the antinodes of the coupling standing-wave field, whereas the phase modulation is provided by the spatial variations of the refractive index.

C. Phase grating

As was mentioned before, the phase gratings have much more diffraction efficiency than the absorption gratings. The essential requirement for inducing a phase grating is the presence of phase modulation, which can be generated by periodically modulating the dispersion of the medium. Figures 4(a)–4(c) show the amplitude and the phase modulations for a Ξ -type, V -type, and ($\Xi+V$)-type atomic systems, respectively. As it can be seen from Fig. 4(a), in the absence of the standing-wave field the periodic change of the amplitude and phase of the transmission function has vanished. On the other hand, in Fig. 4(b) for a V -type system, it is clear that a phase modulation on the order of π is induced across the probe field, whereas a small-amplitude modulation oscillates around $|T(x)| = 1$. In Figs. 4(d)–4(f), the diffraction patterns of the electromagnetically induced phase grating are displayed as a function of $\sin\theta$ for Ξ -type, V -type, and ($\Xi+V$)-type atomic systems, respectively. It is observed that the efficiency of the combined V and Ξ system is larger than that for a simple V or Ξ system. From the grating equation, i.e., $\sin\theta = n\lambda_p/\Lambda_{cx}$, it is predicted that the first and second orders of diffraction take place in $\sin\theta = \pm 0.25$ and $\sin\theta = \pm 0.5$, respectively. In off-resonance condition, i.e., $\Delta_p \neq 0$, for the ($\Xi+V$)-type atomic system, the Rydberg-EIT plays a crucial role in increasing the diffraction efficiency. In this case, large dispersion is accompanied by almost zero absorption, and this implies that we can implement a nearly ideal phase grating. Thus, the probe field energy in the zeroth order of diffraction dramatically decreases due to the increment of the phase modulation, and this energy transfers to the higher orders of diffraction. Therefore one can take advantage of this phenomenon to enhance the efficiency of the all-optical induced phase grating.

As can be seen from the Eq. (7), the diffraction efficiency strongly depends on the interaction length of the atomic sample. Figure 5 shows the variations of the first- and second-order diffraction intensities $I_p(\theta_1)$ (solid line) and $I_p(\theta_2)$ (dotted line) as a function of the interaction length L . When

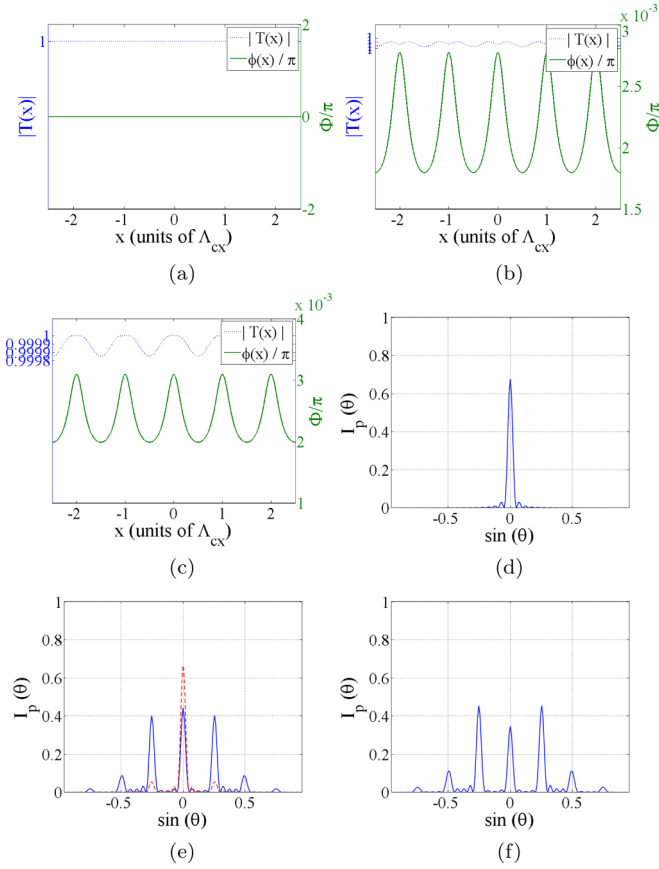


FIG. 4. *Phase grating*: The amplitude $|T(x)|$ and the phase ϕ/π of the transmission function vs x for (a) $\Omega_{c1} = 0$, $\Omega_{c2} = 2\Gamma_2$; (b) $\Omega_{c1} = 1\Gamma_2$, $\Omega_{c2} = 0$; (c) $\Omega_{c1} = 1\Gamma_2$, $\Omega_{c2} = 2\Gamma_2$. (d)–(f) Corresponding normalized diffraction intensity for off-resonance condition, i.e., $\Delta_p = 3\Gamma_2$, $\Delta_{c1} = \Delta_{c2} = 0$. Common parameters are $\Lambda_{cx} = 4$, $M = 5$, and $L = 50$.

the interaction length is small, the probe absorption and the phase modulation are both insignificant. Therefore the probe energy gathers into the zeroth-order direction. Increasing L leads to an enhancement of the phase modulation depth,

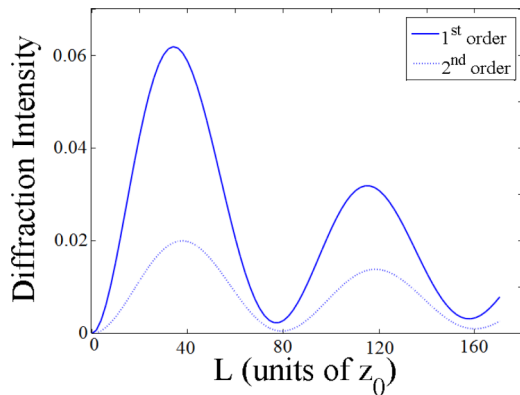


FIG. 5. First-order (solid line) and second-order (dotted line) diffraction intensity in terms of interaction length L for (a) absorption grating (b) phase grating. Common parameters are $\Omega_{c1} = 1\Gamma_2$, $\Omega_{c2} = 2\Gamma_2$, and $\Lambda_{cx} = 4$.

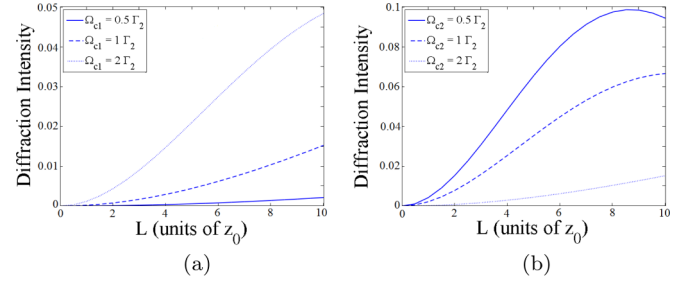


FIG. 6. The first-order diffraction intensity as a function of interaction length L for (a) various coupling field intensities and $\Omega_{c2} = 2\Gamma_2$, (b) various control field intensities and $\Omega_{c1} = 1\Gamma_2$. Common parameters are $\Lambda_{cx} = 4$ and $\Delta_p = \Delta_{c1} = \Delta_{c2} = 0$.

which causes the probe energy to be diffracted into high-order directions. It can be seen that there is an optimal value for interaction length in both cases. For large values of L , the absorption is dominant and therefore the diffraction intensities decrease.

Figures 6(a) and 6(b) show the effect of the Rabi frequency of the coupling and control fields on the first order of diffraction, respectively. It can be observed that increasing the coupling field intensity leads to higher diffraction intensities, while there is an optimum value for intensity of the control field.

The results show that in order to obtain high efficient gratings, optimally choosing the system and laser parameters is very important. Therefore, tuning properly the Rabi frequency of coupling and control as well as the interaction length is a good way to obtain large diffraction efficiencies in both all-optical absorption and phase gratings.

IV. CONCLUSIONS

In summary, we used EIG via Rydberg atoms to generate all-optical diffraction grating. We have studied the electromagnetically induced grating in a four-level $[(V + \Xi)\text{-type}]$ atomic system, including a Rydberg state as the uppermost level. It is found that the control field intensity, the probe field detuning, and the interaction length can improve the Fraunhofer diffraction intensity in the proposed atomic model. Also, it is shown that the large diffraction intensities are achieved both in the first- and second-order directions. Such a system could find applications in novel photonic devices, such as all-optical switches and routers and so on. These results will be of great importance for future experiments relying on knowledge of Rydberg-state energies. In the proposed atomic system, the Doppler shift effect resulting from the thermal motion of the atoms is neglected. As a result, the Rydberg-EIT effect is velocity independent and is determined by the system parameters.

ACKNOWLEDGMENT

This work is supported by the Iran National Science Foundation (INSF) (Grant No. 95839673).

- [1] P. Storey, M. Collett, and D. Walls, *Phys. Rev. Lett.* **68**, 472 (1992).
- [2] G. Alber and P. Zoller, *Phys. Rep.* **199**, 231 (1991).
- [3] T. B. H. Reusch and S. L. Williams, *Rydberg Atoms*, September 1997 (Cambridge University Press, Cambridge, UK, 1998).
- [4] J. Deiglmayr, M. Reetz-Lamour, T. Amthor, S. Westermann, A. de Oliveira, and M. Weidemüller, *Opt. Commun.* **264**, 293 (2006).
- [5] B. Weber, H. P. Specht, T. Müller, J. Bochmann, M. Mücke, D. L. Moehring, and G. Rempe, *Phys. Rev. Lett.* **102**, 030501 (2009).
- [6] N. Henkel, R. Nath, and T. Pohl, *Phys. Rev. Lett.* **104**, 195302 (2010).
- [7] P. Schauß, M. Cheneau, M. Endres, T. Fukuhara, S. Hild, A. Omran, T. Pohl, C. Gross, S. Kuhr, and I. Bloch, *Nature (London)* **491**, 87 (2012).
- [8] G. Pupillo, A. Micheli, M. Boninsegni, I. Lesanovsky, and P. Zoller, *Phys. Rev. Lett.* **104**, 223002 (2010).
- [9] F. Cinti, P. Jain, M. Boninsegni, A. Micheli, P. Zoller, and G. Pupillo, *Phys. Rev. Lett.* **105**, 135301 (2010).
- [10] I. Mourachko, D. Comparat, F. de Tomasi, A. Fioretti, P. Nosbaum, V. M. Akulin, and P. Pillet, *Phys. Rev. Lett.* **80**, 253 (1998).
- [11] J. Lim, H.-G. Lee, and J. Ahn, *J. Korean Phys. Soc.* **63**, 867 (2013).
- [12] T. Vogt, M. Viteau, A. Chotia, J. Zhao, D. Comparat, and P. Pillet, *Phys. Rev. Lett.* **99**, 073002 (2007).
- [13] W. R. Anderson, J. R. Veale, and T. F. Gallagher, *Phys. Rev. Lett.* **80**, 249 (1998).
- [14] A. Fioretti, D. Comparat, C. Drag, T. F. Gallagher, and P. Pillet, *Phys. Rev. Lett.* **82**, 1839 (1999).
- [15] M. Płodzień, T. Sowiński, and S. Kokkelmans, *Sci. Rep.* **8**, 9247 (2018).
- [16] T. Vogt, M. Viteau, J. Zhao, A. Chotia, D. Comparat, and P. Pillet, *Phys. Rev. Lett.* **97**, 083003 (2006).
- [17] J. Honer, H. Weimer, T. Pfau, and H. P. Büchler, *Phys. Rev. Lett.* **105**, 160404 (2010).
- [18] M. Saffman, T. G. Walker, and K. Mølmer, *Rev. Mod. Phys.* **82**, 2313 (2010).
- [19] L.-M. Duan, M. D. Lukin, J. I. Cirac, and P. Zoller, *Nature (London)* **414**, 413 (2001).
- [20] M. Saffman, X. L. Zhang, A. T. Gill, L. Isenhower, and T. G. Walker, *J. Phys.: Conf. Ser.* **264**, 012023 (2011).
- [21] J. Ruseckas, I. A. Yu, and G. Juzeliūnas, *Phys. Rev. A* **95**, 023807 (2017).
- [22] I. Friedler, D. Petrosyan, M. Fleischhauer, and G. Kurizki, *Phys. Rev. A* **72**, 043803 (2005).
- [23] L. E. E. de Araujo, *Opt. Lett.* **35**, 977 (2010).
- [24] P.-W. Zhai, X.-M. Su, and J.-Y. Gao, *Phys. Lett. A* **289**, 27 (2001).
- [25] Y. Zhang, A. W. Brown, and M. Xiao, *Opt. Lett.* **32**, 1120 (2007).
- [26] Y. Zhang, C. Yuan, Y. Zhang, H. Zheng, H. Chen, C. Li, Z. Wang, and M. Xiao, *Laser Phys. Lett.* **10**, 055406 (2013).
- [27] A. W. Brown and M. Xiao, *Opt. Lett.* **30**, 699 (2005).
- [28] A. André, M. Bajcsy, A. S. Zibrov, and M. D. Lukin, *Phys. Rev. Lett.* **94**, 063902 (2005).
- [29] H. Y. Ling, Y.-Q. Li, and M. Xiao, *Phys. Rev. A* **57**, 1338 (1998).
- [30] B. K. Dutta and P. K. Mahapatra, *J. Phys. B* **39**, 1145 (2006).
- [31] F. Bozorgzadeh, M. Sahrai, and H. Khoshshima, *Eur. Phys. J. D* **70**, 191 (2016).
- [32] T. Naseri and R. Sadighi-Bonabi, *J. Opt. Soc. Am. B* **31**, 2879 (2014).
- [33] F. Zhou, Y. Qi, H. Sun, D. Chen, J. Yang, Y. Niu, and S. Gong, *Opt. Express* **21**, 12249 (2013).
- [34] J. Tabosa, A. Lezama, and G. Cardoso, *Opt. Commun.* **165**, 59 (1999).
- [35] M. Mitsunaga and N. Imoto, *Phys. Rev. A* **59**, 4773 (1999).
- [36] A. W. Brown and M. Xiao, *J. Mod. Opt.* **52**, 2365 (2005).
- [37] S. Asghar, Ziauddin, S. Qamar, and S. Qamar, *Phys. Rev. A* **94**, 033823 (2016).
- [38] J. Stanojevic, V. Parigi, E. Bimbard, A. Ourjoumtsev, and P. Grangier, *Phys. Rev. A* **88**, 053845 (2013).
- [39] S. Sevinçli, N. Henkel, C. Ates, and T. Pohl, *Phys. Rev. Lett.* **107**, 153001 (2011).
- [40] V. Bharti and V. Natarajan, *Opt. Commun.* **356**, 510 (2015).
- [41] V. Bharti and V. Natarajan, *Opt. Commun.* **392**, 180 (2017).
- [42] H. R. Hamed, M. Sahrai, H. Khoshshima, and G. Juzeliūnas, *J. Opt. Soc. Am. B* **34**, 1923 (2017).
- [43] H. R. Hamed, M. Sahrai, and H. Khoshshima, *Phys. Wave Phenom.* **26**, 47 (2018).
- [44] M. Piotrowicz, C. MacCormick, A. Kowalczyk, S. Bergamini, I. Beterov, and E. Yakshina, *New J. Phys.* **13**, 093012 (2011).
- [45] B. K. Teo, D. Feldbaum, T. Cubel, J. R. Guest, P. R. Berman, and G. Raithel, *Phys. Rev. A* **68**, 053407 (2003).
- [46] H. Cheng, H. M. Wang, S. S. Zhang, P. P. Xin, J. Luo, and H. P. Liu, *Opt. Express* **25**, 33575 (2017).
- [47] A. K. Mohapatra, T. R. Jackson, and C. S. Adams, *Phys. Rev. Lett.* **98**, 113003 (2007).
- [48] A. Gaj, A. T. Krupp, J. B. Balewski, R. Löw, S. Hofferberth, and T. Pfau, *Nat. Commun.* **5**, 4546 (2014).
- [49] J. Geng, G. T. Campbell, J. Bernu, D. B. Higginbottom, B. M. Sparkes, S. M. Assad, W. P. Zhang, N. P. Robins, P. K. Lam, and B. C. Buchler, *New J. Phys.* **16**, 113053 (2014).
- [50] T. Meng, Z. Ji, D. Su, Y. Zhao, L. Xiao, and S. Jia, *Ann. Phys.* **528**, 512 (2016).